Recent advancements in microtomography

Bert Müller*[a,b]

[a]Biomaterials Science Center, Department of Biomedical Engineering, University of Basel, 4123 Allschwil, Switzerland; [b]Biomaterials Science Center, Department of Clinical Research, University Hospital Basel, 4031 Basel, Switzerland

ABSTRACT

The publications on x-ray imaging with a focus on micro- and nanotomography are becoming more and more interdisciplinary and combine the developments in instrumentation and algorithms with dedicated applications. The current challenges relate to synchrotron radiation sources of the fourth generation, to the establishment of phase contrast in laboratory-based systems, to the sound integration of machine learning into data analysis, to the dissemination of the big data, to the suitable preparation of the objects for tomographic imaging, and to the closer and closer collaboration between the experts, for example to address clinical needs for improving human health. This paper summarizes selected key aspects of the more than 60 contributions in the 15th volume on *Developments in X-ray Tomography*.

Keywords: Computed tomography, phase tomography, microtomography, nanotomography, synchrotron radiation, image analysis, artificial intelligence, multimodal imaging.

1. INTRODUCTION

ULRICH BONSE had a formative impact on the field of X-ray imaging and beyond. The participants of the conference "Developments in X-ray Tomography XV" paid tribute to him, which included a dedicated session [1-4]. ULRICH BONSE has had lasting influence through X-ray interference [5]. He formed the conference series by the conscientious organization and implementation of the first five times - in 2004 and 2006 with the highest and second highest number of proceedings papers, see below.

BONSE's pioneering work in microtomography and phase contrast X-ray imaging is now being extended in one of the plenary talks of the X-Ray, Gamma-Ray, and Particle Technologies track and the related proceedings paper [6]. This contribution covered the spectrum from the first phase CT-data of human brain tissue with the resolution of Purkinje cells to the three-dimensional imaging of entire murine brains with a spatial resolution of about one micrometer. Both the feasibility of three-dimensionally imaging the almost one hundred billion biological cells of an entire human brain *post mortem* as well as the challenges related to brain preparation, data acquisition, reconstruction and dissemination of big data were demonstrated [6]. These developments will create the basis for the three-dimensional visualization of cells in many human organs in health and disease, of microstructures in high-performance engineering materials, and of micrometer-sized features in unique cultural heritage objects related to data of petabyte size.

This proceedings volume contains 64 papers. SPIE's Digital Library lists 46 oral contributions and 14 posters with both presentation and paper, four contributions with paper only, and eight presentation-only oral contributions as well as three posters without related proceedings paper. Figure 1 shows the number of contributions to the conference series "Developments in X-ray Tomography" from 1997 to 2024. The proceedings papers of this year can again be grouped into pillars, *i.e.,* Instrumentation I to V, Algorithms I to IV, and Applications I to IV plus the poster session covering the three pillars. In Sections 2 to 4, the author summarizes his appreciations of the valuable talks/posters and related conference papers.

*bert.mueller@unibas.ch; phone +41 61 207 5430; fax 41 61 207 5499; www.bmc.unibas.ch

Developments in X-Ray Tomography XV, edited by Bert Müller, Ge Wang,
Proc. of SPIE Vol. 13152, 131521E · © 2024 SPIE
0277-786X · doi: 10.1117/12.3021765

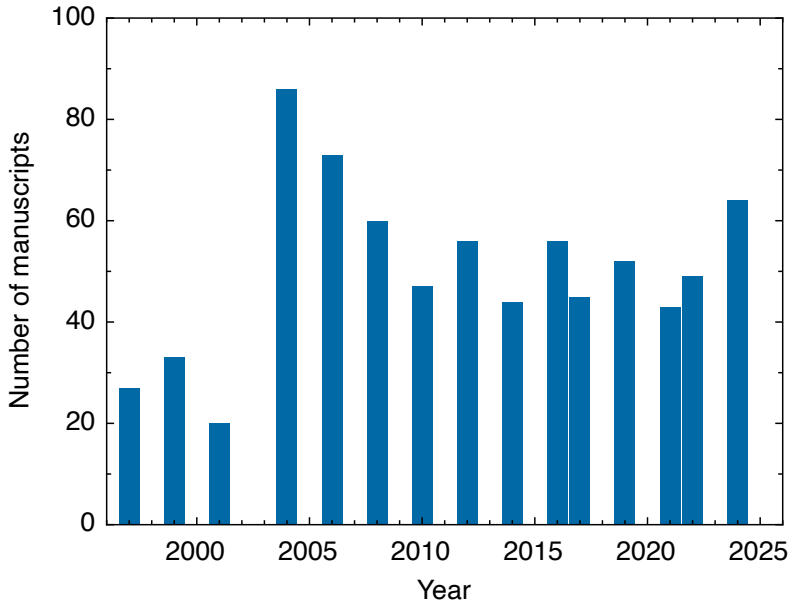

Figure 1. The SPIE volumes of the conference series *Developments in X-ray Tomography* contain an average number of about 50 peer-reviewed papers. This year, 84 oral and poster contributions were accepted. Unfortunately, four contributions were withdrawn and three posters were not presented. Four conference papers had to be rejected, but still 64 papers could be published in the volume 13152, which has been the highest number since 2006.

2. EVOLUTION OF INSTRUMENTATION FOR X-RAY TOMOGRAPHY

2.1 Phase tomography and non-cylindrical objects

Pei-Tzu Lee and coworkers presented a system, which combined synchrotron radiation-based laminography and fluorescence imaging for dedicated geometries of specimens, including flat mouse bone sections and brain tissue slices [7]. This non-destructive multimodal technique, implemented at beamlines 2-BM and 2-ID-E of the Advanced Photon Source at Argonne National Laboratory, provided detailed information on both the interior microstructure and the elemental distribution.

A team from Belgium performed a simulation study using a phantom with aluminum and polymer cylinders of preselected sizes [8]. Implementing gratings with trapezoid shape, they claimed to generate a multiresolution setup by adapting the grating period.

Laboratory-based microtomography systems have been steadily improved. A characteristic example is given by experts from the University College London [9], using molybdenum and copper targets with emission in two directions. This setup allowed simultaneous experiments with millimeter and centimeter fields of view. The authors showed attenuation-contrast data of bamboo and chicken bones as well as phase and dark-field images. Charlotte K. Hagen used the setup from the University College London and listed a few recent examples of instrument improvement [10]. The invited contribution focused on the optimization of data acquisition and discussed the role of the aperture width, cycloidal computed tomography, and under-sampling issues [11].

2.2 Multiscale tomography

At the wiggler-based tomography setup of Biomedical Imaging and Therapy Beamlines of the Canadian Light Source, an efficient detection system for *in vivo* experiments was implemented with effective pixel sizes between 2 and 22 µm and a centimeter-sized field of view [12]. The acquired data could be reconstructed on-the-fly, which was extremely helpful for studies with living animals.

A team from Japan built a synchrotron radiation-based multiscale tomography system, allowing spatial resolution to be changed from 1,000 to 100 nm within three minutes [13]. The full-field microscope using a Fresnel zone plate is designed for photon energies between 7 and 15 keV and a field of view of 60 µm. At the beamline BL20XU of SPring-8 in Japan the users could select between three tomography setups, i.e. microtomography with a beam diffuser in the optical path to get a 6 mm-wide field of view and voxel sizes of 3 µm, microtomography with 1 mm-wide field of view and voxel sizes of 0.5 µm, and nanotomography with a Fresnel-zone-plate-based full-field microscope to reach voxel sizes well below 100 nm. The unique feature is the ability to change magnification within one minute while keeping the specimen on the stage of the manipulator [14].

2.3 Advanced laboratory-based CT systems

Using the Xradia 610 Versa (Carl Zeiss X-ray Microscopy, Inc., Dublin, California, United States) a Swiss team showed images of a mosquito with voxel sizes as small as 180 nm [15]. The external structures resembled electron microscopy pictures, but tomography even allowed the quantification of the internal structures. As example, a single lens of the compound eye was segmented and a focal length of 22 µm determined. Thus, these results showcased the capability of laboratory-based phase tomography for soft tissues, previously achievable only at synchrotron radiation facilities.

With the Exciscope Polaris instrument, a Swedish team extended the field of view in horizontal direction [16]. The mechanics was stable and precise enough to automatically stitch projections so that slices with more than 100 Mpixels and tomographic data with several TB could be reconstructed. Feasibility was demonstrated for a coffee capsule with 3.4 µm-wide voxels and wood with 0.6 µm-wide voxels.

Usually fast tomography is only available at synchrotron radiation facilities. H. Allan and team, however, showed that a laboratory-based source also permitted microCT of simple objects within about one second [17]. Feasibility was demonstrated using an expanding foam.

Laboratory-based tomography has reached a spatial resolution of about 100 nm even without X-ray optics: A team from Munich, Germany, combined a liquid-metal source with a photon counting detection system to obtain nano-tomography data of biological specimens [18].

2.4 Advanced tomographic techniques

A Swiss team performed *in vivo* studies on mouse heads using the beamline ID 17 at the European Synchrotron Radiation Facility, Grenoble, France [19]. They developed a method to detect local displacements in the mouse brain induced by breathing and the pulsative blood flow. Combined with the acquired data, the method allowed the detection of displacements with an amplitude of three micrometers.

A German team combined the Talbot array illuminators as a speckle pattern with the unified modulated pattern analysis as the phase retrieval method and implemented the method at PETRA III beamlines P05 and P07, Hamburg, Germany [20]. They showed quantitative phase tomograms of resorbable bone implants with surrounding bone and an interface layer and paraffin-embedded lymph nodes in ethanol. The results indicated an improvement of the contrast-to-noise ratio by almost a factor of two.

An international team acquired full-field and local tomography data of the human heart, brain, and kidney immersed in a mixture of ethanol and crushed agar gel [21]. The full-field data were recorded with an effective voxel size down to 17 µm. The local tomography data were recorded with 2 µm-wide voxels. The reconstructed data volumes ranged from 0.1 to 15 TB.

The Advanced Photon Source upgrade project included the full-field imaging beamlines 2-BM, 7-BM, and 32-ID. The team from Argonne National Laboratory presented the expected parameter improvements for full-field micro- and nano-tomography user experiments [22].

At the SPring-8 beamline BL28B2 tomography experiments with a photon energy of 200 keV could be performed in an automatic fashion [23]. The maximum field of view was 48 mm in width and 1.2 mm in height. A conventional lithium-ion battery was imaged with a voxel size of 3.7 µm.

It is a challenge to use tomography for imaging large objects such as the human brain with true micrometer resolution, because the field of view does not allow for full-field tomography. Efficient stitching in combination with sub-micrometer mechanical stability and reproducibility of the translation/rotation stages was proposed [24]. The presented results demonstrated the feasibility to obtain tomography data of an entire human brain with a spatial resolution of about 3 μm.

2.5 Multimodal imaging and advanced detector technology

X-ray-based luminescence computed tomography was used to determine the oxygen concentration within an agar phantom [25]. For this purpose, the authors used photons of two wavelengths. They plan to apply an improved version of the technology to measure the local oxygen concentrations in mouse bone marrow.

Using a conventional X-ray source, a team from Beijing proposed the simultaneous detection of transmitted photons for CT imaging and of scattered and fluorescence photons from a poly(methyl methacrylate) object 3 cm in diameter [26]. This object contained cylinders homogeneously filled with water or a 5 mg/mL gadolinium solution, six of them 6 mm in diameter and four of them 3 mm in diameter. Proof of concept was presented using simulations and experiments.

A relevant equipment component for live mouse imaging using microCT and optical microscopy is the suitable holder. A 3D-printed table proposed by a team from the United States allowed for the comfortable, imaging-compatible animal bedding with heating capability [27].

Using a conventional lithium ion battery, the benefit of combining neutron and X-ray microtomography was demonstrated [28]. This approach included a simultaneous analysis of the obtained data with the aim to identify defects before, during and after usage.

The P07 beamline at Petra III, Hamburg, Germany allowed for the combination of X-ray diffraction contrast tomography and conventional synchrotron radiation-based microtomography [29]. The performance of this three-dimensional imaging combination was demonstrated for partially resorbed magnesium-titanium implants with the surrounding bone of rat tibiae.

Detectors for X-ray fluorescence computed tomography suffer from multi-pixel events. A team from Beijing proposed a method to correct such multi-pixel events and validated the idea using a phantom with gadolinium solutions of 0.0, 0.2, 0.5, 0.8, and 1.0 mg/mL [30].

A tomographic nuclear imaging system based on a Compton camera without a mechanical collimator was presented [31]. Simulations gave an idea of the efficiency and the image quality. Experimental results of a very simple phantom confirmed the value of the approach.

The direct comparison of scanning acoustic microscopy and three-dimensional X-ray imaging was used to physically inspect integrated circuit packaging [32]. The authors discussed the potential of artificial intelligence for improved defect detection in integrated circuits and their connections. The potential benefits in combining scanning acoustic microscopy and microCT were evaluated for the inspection of integrated circuit packaging [33].

3. ALGORITHMS FOR TOMOGRAPHIC IMAGING AND IMAGE ANALYSES

3.1 Artifact correction and denoising

A pipeline for denoising interior photon-counting computed tomography was proposed [34]. To become independent on the lengthy iterative reconstruction process, the authors introduced a neural network to remove artifacts from the back projection of a truncated sinogram [35].

Deep neural network-based strategies for improving photon counting computed tomography combining image and sinogram domain were evaluated [36]. Using a Wasserstein generative adversarial network as framework for detector correction, the authors carefully evaluated the effectiveness of pre-trained and training-from-scratch convolutional neural networks as perceptual loss functions to address charge splitting and pulse pileup corrections in photon counting computed tomograms.

Using the example of sandstone imaging, a team from a company based in California demonstrated that their method for image restoration with a synthetic prior intermediate provided better results than legacy reconstruction and state-of-the-art deep learning reconstruction [37].

Focal spot drifts adversely affected the projections especially in grating-based tomography setups. In order to reduce the related artifacts, a simulation-based method for flat-field correction was presented [38].

3.2 Deep reconstruction and image analysis

Planar structures such as wafer-level integrated circuits have been a challenge for computed tomographic imaging and generally benefit from laminography. On the basis of a self-supervised deep image restoration workflow as part of laminographic tomography one could rapidly inspect and analyze failures in integrated circuits packaging [39].

Battery characterization studies have been often based on three-dimensional imaging and related data analysis. Employing a Zeiss Xradia Versa 630 with a Mark IV source and a pixel length of 1.5 μm, spatial resolution and especially contrast with reduced noise could be improved by deep-learning-based reconstructions [40].

An impressive example for the adaptation of neural networks for segmenting tissues in mice was presented by a team from Illinois. This team has collected a huge number of synchrotron radiation-based CT data (beamlines 2-BM-B and 5-BM-C at the Advanced Photon Source) and segmented the mineralized jaw tissues from a range of mouse phenotypes [41]. This quantification was only possible by automatic procedures, here by the implementation of convolutional neural networks.

A team from Florida suggested a workflow to combine machine learning algorithms and fundamental physical principles with the aim to improve reconstruction even if projections are missing [42].

3.3 Tomographic reconstruction

A comprehensive, multi-author contribution related to an open-source framework for real-time X-ray image simulation that could be validated across numerous applications ranging from educational purposes via scanner development in computed tomography to machine learning for three-dimensional image analysis [43]. Its versatility and accuracy enabled practical uses in optimization problems and radiographic analysis across several fields of application.

In order to expand the field of view in the reconstructed phase data, a multi-frame approach for phase retrieval by means of the unified modulated pattern analysis model was presented [44]. The feasibility of the approach was proven by three-dimensional imaging of human placental tissue.

A specific approach based on a static, multi-source CT system for cargo inspection was presented in detail [45]. The authors from Belgium and France dealt with the combination of limited views and the scarcity of training data and, therefore, proposed the application of deep image prior.

The acquisition, reconstruction, and analysis of time-resolved and high-resolution data of the academic and industrial users from synchrotron radiation-based tomography has been a challenge. Thus, a team from northern Germany explored machine learning approaches for the reconstruction, processing, and analysis of synchrotron radiation-based tomography data of the beamlines P05 and P07 at the storage ring PETRA III, Hamburg, Germany [46]. They applied supervised learning for multimodal data analysis to generate virtual histology in three dimensions for resorbable bone implants.

On-the-fly data acquisition is an established technique for time-efficient tomography and is frequently used at synchrotron radiation facilities. In specific cases, non-uniform angular velocity might be beneficial. A Belgium team extended the established reconstruction algorithms for constant sample rotation and included a generalized motion model [47].

3.4 Sophisticated X-ray tomography

The Helmholtz-Zentrum Hereon, Germany, operates microtomography systems at the beamlines P05 and P07 using the synchrotron radiation of the storage ring PETRA III at DESY, Hamburg, Germany. A team of beamline scientists listed the hardware requirements and the calibration protocols used [48]. They adjusted the preprocessing pipeline to the limits

of the mechanical stability of the sample manipulator with the aim of stitching projection data for high spatial resolution and large object volumes. This hardware together with the dedicated software was also used to validate the feasibility of acquiring an entire human brain *post mortem* with a voxel size of 2.5 µm [24].

For synchrotron radiation-based tomographic imaging of large volumes at relative high resolution, projection stitching is suitable, as long as the mechanical stability of specimen and instrumentation is given for the recording duration, typically hours. A Swiss team showed that the preferred tiling scheme with respect to acquisition time and dose efficiency depended on the angular sampling requirements for local tomography [49]. If the number of projections was chosen independent of the total object width, reconstruction tiling was faster, as demonstrated for a 2 cm-wide brain sample and an effective voxel size of 0.65 µm.

Partial volume phenomena in computed tomography can occur due to the general choice of cubic voxels. A team from Antwerp reconstructed data of a gear phantom using a tetrahedral mesh in a memory efficient fashion [50]. They extended the graphics processing unit-accelerated iterative reconstruction technique to solve the inverse problem on tetrahedra.

Fast detection systems could reconstruct data on-the-fly. At the FaXToR beamline of the Spanish synchrotron ALBA such capabilities had become available [51]. The related hard- and software will be further refined with the aim to reach a throughput of 10 GB/s and the sub-second volume visualization.

4. SELECTED APPLICATIONS OF ADVANCED COMPUTED TOMOGRAPHY

4.1 Micro- and nano-tomography in biomedicine

A Swiss team imaged the auditory system extracted from a donated human body [52]. With the fast tomography setup at the TOMCAT beamline of the Swiss Light Source, they detected vibration-induced micromotions. The displacement magnitudes were just a few micrometers - a value just below the limits of the spatial resolution. Another tomography study of the auditory system showed the impact of noise in mice [53]. Using the ANATOMIX beamline at the Synchrotron SOLEIL, Saint-Aubin, France, thousands of hair cells of the decalcified, paraffin-embedded cochleae could be semi-automatically detected. The found difference between low and high sound levels could be validated on the same cochleae by immunofluorescence microscopy and histology. Impressive three-dimensional data of inner ear of harbor porpoise with voxel sizes of 2.5 µm were recorded at the high-energy materials science beamline P07 at the storage ring PETRA III, Hamburg, Germany [54]. The experimentalists used an asymmetric rotation axis and five vertical scans to cover the whole decalcified inner ear.

Fully three-dimensional virtual histology of physically soft tissues is not restricted to synchrotron radiation facilities but also has been developed at laboratory-based tomography setups. A team from Munich enhanced the approach by developing and applying dedicated stains [55]. The power of the approach was demonstrated for pituitary and adrenal glands of healthy and diseased rats *post mortem*. Correlating tomography data and subsequently obtained histology slides of the same object, one could color the tomography data according to the colors of the selected stain. Such an approach in combination with machine learning was presented [56]. The team validated the method by generating artificially stained virtual histology datasets from bone explants.

Rehydrated human corneas were immersed in Lugol's iodine to enhance the contrast-to-noise ratio especially of the cells in the epithelium and endothelium [57]. The effect of contrast enhancement was quantified employing the laboratory-based microCT-system Bruker Skyscan 2211.

Laboratory-based microCT systems proved suitable for the visualization of the palatal anatomy and the micro-architecture of unstained human skeletal muscle tissue [58], but synchrotron radiation-based microtomography provided additional soft-tissue contrast owing to phase retrieval. It allowed manual segmentation of muscle segments in a plasticized specimen. These results indicated that minimal incision palatoplasty with preservation of the hamular region is advantageous in the surgery of cleft palate to preserve velopharyngeal and Eustachian tube function.

4.2 Non-destructive characterization of dedicated objects

A team from Norway developed a protocol for contrast-enhanced microtomography to visualize soft tissues and cells in the direct neighborhood to bone [59]. To validate the procedure, decalcified murine femurs were stained with iodine and tungsten, respectively, and imaged at the SYRMEP beamline of the synchrotron laboratory ELETTRA, Trieste, Italy.

With probably over two billion objects in the collection-holding institutions of the world to be nondestructively transformed into three-dimensional data, a huge fundus for microtomography has been identified. A Swiss team showed an impressive selection of these unique objects, which were three-dimensionally visualized by means of laboratory-based microCT systems [60]. Related renderings of the unique objects were presented.

4.3 Imaging multicomponent objects

A German team investigated composite failure by mechanically loading a NiTi-wire embedded into an epoxy resin [61]. *In situ* pull-out tests by stepwise loading increase were performed at the tomography setup of the beamline P07 at the storage ring PETRA III, Hamburg, Germany. The preliminary results indicated that interfacial failure was not only shear-stress-induced. Normal strain due to transverse contraction of the shape memory alloy wire also played a role.

A team from Florida applied computed tomography and optical microscopy to characterize electronic devices and their connections [62]. From the top and bottom layer microscopy as well as from the CT layers, they extracted features for a correlated segmentation of the components.

A team from the United States visualized the abdominal vertebral centrum from a great hammerhead shark under compressive load with microCT at the beamline 8.3.2 of the Advanced Light Source [63]. The authors could demonstrate that the shark intermediale trabeculae underwent substantial deflections in response to physiologically relevant compression. This non-uniform response might relate to the microstructural anisotropy.

4.4 Advanced tomographic imaging

Subcellular structures can be segmented from microCT data even in an automatic fashion [64]. Mouse brain data from the beamline ID16A at the European Synchrotron Radiation Facility in Grenoble, France, allowed automatic cell nuclei segmentation [65]. The authors could show that several ten thousand nuclei per dataset were reliably identified.

The Diamond I13L beamlines located near Oxford in UK served for tomographic imaging of many porous structures even under dynamic conditions [66]. The authors provided a series of life science examples and elucidated the science impact of the Diamond II upgrade.

5. CONTINUOUS DEVELOPMENTS IN THE FIELD OF TOMOGRAPHY

The synchrotron radiation facilities have generally made micro- and nano-tomography setups available for the international users. Related developments on the detection systems have been integrated into cutting-edge laboratory-based microCT systems that now reached voxel sizes smaller than 200 nm. Fast tomographic and low-contrast imaging as well as living animal studies are still mainly studied at synchrotron radiation facilities, but are also more and more often addressed by advanced laboratory-based systems, which include liquid metal jet X-ray sources.

The numerous tomography systems have provided a huge amount of data to be stored and treated. The big data can only be efficiently treated in an automatic fashion – more and more often with machine learning tools. Their dissemination among the interested community is a major challenge, as pointed out by the participants of the SPIE conference “Developments in X-ray Tomography XV”.

The fields of applications are steadily broadened and include some foci such as the billion unique objects from cultural heritage as well as animal and human tissues for diagnostic purposes. Hard X-ray tomography is often complementary to other imaging techniques. The uniqueness of tomography lies (i) in the tuneability of the photon energy, (ii) in the almost isotropic spatial resolution in the three-dimensional space, and (iii) in the multiple contrast mechanisms including phase contrast.

ACKNOWLEDGEMENT

The author gratefully acknowledges the valuable input of Stuart R. Stock and Ge Wang.

REFERENCES

[1] Müller, B., "Tribute to Ulrich Bonse: His doctoral thesis on x-ray imaging of strain fields around dislocations in germanium single crystals," Proc. SPIE **13152**, 131521F (2024).

[2] Stock, S. R., "Ulrich Bonse's impact on development of x-ray tomography," Proc. SPIE **13152**, 131521G (2024).

[3] Momose, A., "Bonse-Hart x-ray interferometer and tomography," Proc. SPIE **13152**, 131521H (2024).

[4] Beckmann, F., "Tribute to Ulrich Bonse: full-field imaging using first to third generation of synchrotron radiation sources," Proc. SPIE **13152**, 131521I (2024).

[5] Wang, G., "Ulrich Bonse's lasting influence through x-ray interference," Proc. SPIE **13152**, 131521J (2024).

[6] Müller, B., "On the cusp of x-ray tomographic mapping of the human brain and its 10^11 cells," Proc. SPIE **13152**, 1315202 (2024).

[7] Lee, P.-T., Marin, F. S., Nikitin, V. V., and Antipova, O. A., "An innovative integration of high-resolution synchrotron x-ray laminography fluorescence imaging," Proc. SPIE **13152**, 1315207 (2024).

[8] Vanthienen, P.-J., Francken, N., Sijbers, J., and De Beenhouwer, J., "Multi-resolution gratings for edge illumination x-ray phase contrast imaging: A simulation study." Proc. SPIE **13152**, 1315208 (2024).

[9] Roche i Morgó, O., Jia, Y., Allan, H., Doherty, A., Navarrete-León, C., Astolfo, A., Jiang, L., Ferrara, J. D., and Endrizzi, M., "A new user facility with flexible multi-scale, multi-contrast micro-CT capabilities," Proc. SPIE **13152**, 1315209 (2024).

[10] Hagen, C. K., Lioliou, G., Roche i Morgó, O., Shah, K., Zekavat, A., Astolfo, A., Munro, P. R. T., Cipiccia, S., Endrizzi, M., and Olivo, A., "X-ray micro-computed tomography with amplitude modulated beams (beam tracking, edge illumination): opportunities, challenges, and outlook," Proc. SPIE **13152**, 131520A (2024).

[11] Lioliou, G., Charman, A., Roche i Morgó, O., Endrizzi, M., Arridge, S., Bate, D., Olivo, A., and Hagen, C., "Nyquist-compliant cycloidal computed tomography," Physical Review Applied **22**(3), 034011 (2024).

[12] Gasilov, S., Rochet, X., Panahifar, A., and Cooper, D. M. L., "New high-numerical-aperture macroscope for low radiation dose tomography at the BMIT Beamlines of the Canadian Light Source," Proc. SPIE **13152**, 131520F (2024).

[13] Uesugi, K., Yasutake, M., and Takeuchi, A., "Development of micro/nano-tomography system at SPring-8 BL47XU," Proc. SPIE **13152**, 131520G (2024).

[14] Takeuchi, A., Uesugi, M., Sada, Y., and Uesugi, K., "Hierarchical three-dimensional imaging using x-ray micro-/nano-tomography at BL20XU of SPring-8," Proc. SPIE **13152**, 131521R (2024).

[15] Schulz, G., Spörri, E., Gschwind, M., Deyhle, H., and Müller, B., "Non-destructive imaging of internal structures of a mosquito with sub-micrometer resolution," Proc. SPIE **13152**, 131520M (2024).

[16] Twengström, W., Larsson, J. C., Gidén, T., Allner, S., and Willner, M., "Horizontal extension of the field-of-view in cone-beam tomography at a laboratory instrument," Proc. SPIE **13152**, 131520N (2024).

[17] Allan, H., Roche i Morgó, O., Navarrete-Leon, C., Jia, Y., and Endrizzi, M., "Sub-second dynamic x-ray micro-CT and fast phase-sensitive multi-contrast micro-CT with a laboratory source," Proc. SPIE **13152**, 131520O (2024).

[18] Ilg, P., Schurius, O., Dierolf, M., Günther, B., and Pfeiffer, F., "Improvements of a laboratory phase-contrast nano-computed tomography system," Proc. SPIE **13152**, 131521U (2024).

[19] Humbel, M., Girona Alarcón, M., Kuo, W., Spera, I., Bausch, B., Fardin, L., Deyhle, H., Rodgers, G., Engelhardt, B., Proulx, S., Kurtcuoglu, V., Müller, B., and Tanner, C., "Detection of cardiac-induced motion in murine

cerebrospinal fluid space captured in vivo with synchrotron radiation-based microtomography," Proc. SPIE **13152**, 1315214 (2024).

[20] John, D., Riedel, M., Gustschin, A., Savatović, S., Breit, A., De Marco, F., Bidola, P., Hammel, J. U., Moosmann, J., Wieland, D. C. F., Berit, Z.-P., B., Beckmann, F., and Herzen, J., "Recent developments in quantitative phase-contrast microtomography using Talbot Array Illuminators," Proc. SPIE **13152**, 1315215 (2024).

[21] Brunet, J., Walsh, C. L., Tafforeau, P., Dejea, H., Cook, A. C., Bellier, A., Engel, K., Jonigk, D. D., Ackermann, M., and Lee, P. D., "Hierarchical phase-contrast tomography: a non-destructive multiscale imaging approach for whole human organs," Proc. SPIE **13152**, 1315216 (2024).

[22] Mittone, A., Nikitin, V., Clark, S. J., Deriy, A., Fezzaa, K., Kastengren, A., Shevchenko, P., and De Carlo, F., "Full field micro and nano tomography at APS-U," Proc. SPIE **13152**, 1315217 (2024).

[23] Uesugi, K., Hoshino, M., Uesugi, M., Kameshima, T., Hatsui, T., Joti, Y., Hiraki, T., Honma, T., Yamada, J., Sugahara, M., Takano, H., and Yabashi, M., "Development of fully automatic high energy x-ray tomography system at SPring-8 BL28B2," Proc. SPIE **13152**, 131521S (2024).

[24] Humbel, M., Beckmann, F., Moosmann, J., Deyhle, H., Schulz, G., Tanner, C., Rodgers, G., and Müller, B., "A tomography slice through the entire human brain with less than three micrometer voxels," Proc. SPIE **13152**, 1315220 (2024).

[25] Zhang, Y., Fang, Y., Abbaraju, V., Anker, J. N., Cong, W., Wang, G., and Li, C., "Oxygenation imaging of deep targets at high resolution with an x-ray luminescence micro-CT system," Proc. SPIE **13152**, 1315218 (2024).

[26] Li, L., Song, J., and Pu, S., "Full-field multimodal imaging technology of x-ray transmission, fluorescence, and scattering tomography (PI-CT) with polychromatic source," Proc. SPIE **13152**, 131521A (2024).

[27] Xue, W., Liang, Y., Li, M., Gao, S., Intes, X. R., and Wang, G., "A 3D-printed table for hybrid x-ray CT and optical imaging of a live mouse," Proc. SPIE **13152**, 131521L (2024).

[28] Son, J., Kim, D., Won, J., Heo, Y., Kim, J., Kim, T. J., Lee, J. M., and Lee, S. W., "Feasibility test of simultaneous neutron and x-ray tomography for HANARO thermal neutron beam line," Proc. SPIE **13152**, 131521N (2024).

[29] Lottermoser, L., Beckmann, F., Moosmann, J., Garamus, V. M., Iskhakova, K., Zeller-Plumhoff, B., and Wieland, F., "Parallel usage of x-ray diffraction contrast tomography and micro-computed tomography for multi-modal characterization at the HEMS P07 beamline," Proc. SPIE **13152**, 131521T (2024).

[30] Pu, S., Song, J., and Li, L., "A study on position and energy correction of multi-pixel events in pixelated semiconductor detector for XFCT imaging," Proc. SPIE **13152**, 131521V (2024).

[31] Liang, Y., Li, M., Han, S., Yu, H., and Wang, G., "SPECT with a Compton camera for thyroid cancer imaging," Proc. SPIE **13152**, 1315224 (2024).

[32] Varshney, N., Ghosh, S., Craig, P., Kottur, H. R., Dalir, H., and Asadizanjani, N., "Challenges and opportunities in non-destructive characterization of stacked IC packaging: insights from SAM and 3D x-ray analysis," Proc. SPIE **13152**, 1315225 (2024).

[33] Craig, P., Varshney, N., Roy, A., Woychik, C., Dalir, H., and Asadizanjani, N., "Motivating automated multimodal failure analysis for heterogeneously integrated devices," Proc. SPIE **13152**, 1315228 (2024).

[34] Tanveer, M. S., Wiedeman, C., Li, M., Shi, Y., De Man, B., Maltz, J. S., and Wang, G., "Deep-silicon photon-counting x-ray projection denoising through reinforcement learning," Journal of X-Ray Science and Technology **32**, 173-205 (2024).

[35] Tanveer, M. S., Wiedeman, C., Shi, Y., Yu, H., and Wang, G., "Interior photon-counting CT data denoising via multi-agent reinforcement learning," Proc. SPIE **13152**, 131520C (2024).

[36] Morovati, B., Li, M., Han, S., Xu, Y., Zhou, L., Wang, G., and Yu, H., "Impact of network architecture and training strategy for photon counting CT data correction," Proc. SPIE **13152**, 131520D (2024).

[37] Andrew, M., Andreyev, A., Yang, F., Xu, M., and Xu, S., "X-ray reconstruction using synthetic prior image restoration, with application to noise and artefact removal," Proc. SPIE **13152**, 131520E (2024).

[38] Keklikoğlu, D. G., Francken, N., Huyge, B., Merdan, Z., De Beenhouwer, J., and Sijbers, J., "Dynamic flat field correction in edge illumination imaging," Proc. SPIE **13152**, 131521P (2024).

[39] Xu, S., Candell, S., Case, T., Göhnermeier, A., Irwin, J., Majlan, K., Preil, M., Ruoff, J., Xu, M., Yang, F., and Andrew, M., "Self-supervised deep image restoration for x-ray computed laminographic tomography," Proc. SPIE **13152**, 131520T (2024).

[40] Johnson, N. S., Trenikhina, Y., Bale, H., and Kelly, S., "Deep-learning models enable high-resolution reconstruction of large-volume x-ray microscopy datasets," Proc. SPIE **13152**, 131520U (2024).

[41] Cooley, V., Suwandi, E., Stock, S. R., and Joester, D., "Adapting neural networks for rapid segmentation of mineralized tissues in mouse jaws," Proc. SPIE **13152**, 131520V (2024).

[42] Ghosh, S., Varshney, N., Al Hasan, M. M., Roy, A., Craig, P., Koppal, S. J., Dalir, H., and Asadizanjani, N., "Exploring physics-informed machine learning for system matrix formulation in x-ray imaging forward models," Proc. SPIE **13152**, 131521W (2024).

[43] Vidal, F. P., Afshari, S., Ahmed, S., Atkins, C., Béchet, E., Bellot, A. C., Bosse, S., Chahid, Y., Chou, C.-Y., Culver, R., Dixon, L., Friemann, J., Garbout, A., Hatton, C., Henry, A., Leblanc, C., Leonardi, A., Létang, J. M., Lipscomb, H., Manchester, T., Meere, B., Middleburgh, S., Mitchell, I., Perera, L., Puig, M., and ugwell-Allsup, J., "X-ray simulations with gVXR as a useful tool for education, data analysis, set-up of CT scans, and scanner development," Proc. SPIE **13152**, 131520W (2024).

[44] Savatović, S., De Marco, F., Riedel, M., Laundon, D. J., Regner, M.-L., Hammel, J. U., Lewis, R. M., Herzen, J., and Thibault, P., "Extending the field-of-view of speckle-based microtomography with the UMPA model," Proc. SPIE **13152**, 131520X (2024).

[45] Bossuyt, C., den Dekker, A. J., Iuso, D., Hoang, T., Escoda, J., Costin, M., Sijbers, J., and De Beenhouwer, J., "Deep image prior for sparse-view reconstruction in static, rectangular multi-source x-ray CT systems for cargo scanning," Proc. SPIE **13152**, 131520Y (2024).

[46] Moosmann, J., Ahrens, J., Irvine, S., Wong, T. M., Lucas, C., Beckmann, F., Hammel, J. U., Wieland, D. C. F., Zeller-Plumhoff, B., and Heuser, P., "Machine learning for the reconstruction and analysis of synchrotron-radiation tomography data," Proc. SPIE **13152**, 131520Z (2024).

[47] Huyge, B., Renders, J., De Beenhouwer, J., and Sijbers, J., "X-ray image reconstruction for continuous acquisition with accelerated rotation," Proc. SPIE **13152**, 131521Y (2024).

[48] Beckmann, F., Moosmann, J., Hammel, J. U., and Wilde, F., "Intensity-based stitching microtomography using synchrotron radiation at DESY," Proc. SPIE **13152**, 1315210 (2024).

[49] Humbel, M., Tanner, C., Rodgers, G., Deyhle, H., Schulz, G., and Müller, B., "Comparison of large-volume imaging approaches using computed tomography," Proc. SPIE **13152**, 1315211 (2024).

[50] Merckx, J., den Dekker, A. J., De Beenhouwer, J., and Sijbers, J., "Fast and efficient tetrahedral volume mesh reconstruction with CAD-ASTRA," Proc. SPIE **13152**, 1315212 (2024).

[51] Jover-Mañas, G., Cova, F., Bouffetier, V., Wohl, S., Quintana, J. S., Heras, P. C., Soler, N., and Patera, A., "High-throughput x-ray microtomography at FaXToR: a survey towards high performance image reconstruction," Proc. SPIE **13152**, 1315213 (2024).

[52] Schmeltz, M., Ivanovic, A., Schlepütz, C. M., Wimmer, W., Anschuetz, L., and Bonnin, A., "High-resolution dynamic synchrotron-based x-ray microtomography of the human middle ear," Proc. SPIE **13152**, 1315203 (2024).

[53] Levano, S., Tanner, C., Schulz, G., Horber, R., Weitkamp, T., Müller, B., and Bodmer, D., "Evaluation of the noise-exposed cochlea using synchrotron radiation-based microtomography," Proc. SPIE **13152**, 1315204 (2024).

[54] Rojas, L., Moosmann, J., Beckmann, F., Moysan, L., Siebert, U., IJsseldijk, L. L., Fiedler, I. A. K., Busse, B., and Morell, M., "Suitability of synchrotron-radiation phase-contrast tomography for imaging of inner ear of harbor porpoise," Proc. SPIE **13152**, 1315223 (2024).

[55] Petzold, L. M., Busse, M., Mohr, H., Pellegata, N. S., Pfeiffer, F., and Herzen, J., "Development of a H&E multi-agent-staining method for laboratory-microCT applied to endocrine glands of MENX rats," Proc. SPIE **13152**, 1315205 (2024).

[56] Irvine, S., Lucas, C., Bootbool, M., Galli, S., Zeller-Plumhoff, B., and Moosmann, J., "Multi-modal image registration and machine learning for the generation of 3D virtual histology of bone implants," Proc. SPIE **13152**, 131521Z (2024).

[57] Hildebrand, T., Boix-Lemonche, G., Haugen, H. J., Petrovski, G., and Nogueira, L. P., "Contrast-enhanced micro-CT for visualization of cell distribution in hydrated human cornea," Proc. SPIE **13152**, 1315221 (2024).

[58] Schönegg, D., Deyhle, H., Schulz, G., Tanner, C., Ahmed, S., Atwood, R., Mueller, A. A., Müller-Gerbl, M., Mezey, S., Lieber, R. L., Khounsary, A., and Müller, B., "Three-dimensional hard x-ray micro-tomographic imaging of the human palatal anatomy and gracilis muscle," Proc. SPIE **13152**, 1315229 (2024).

[59] Hildebrand, T., Ma, Q., Heyward, C. A., Haugen, H. J., and Nogueira, L. P., "Advanced soft tissue visualization in conjunction with bone structures using contrast-enhanced micro-CT," Proc. SPIE **13152**, 131520J (2024).

[60] Costeur, L., Friesenhagen, T., and Schulz, G., "X-ray microtomography of fossil types in natural history collections," Proc. SPIE **13152**, 131521D (2024).

[61] Gurka, M., Jungbluth, J., Bruns, S., Beckmann, F., and Moosmann, J., "In-situ synchrotron CT measurements on the interface between shape memory alloy wire and polymer matrix in hybrid composites under tensile loading," Proc. SPIE **13152**, 131520P (2024).

[62] Craig, P., Varshney, N., Roy, A., Ghosh, S., Patil, C., Dalir, H., and Asadizanjani, N., "Multi-modal printed circuit board netlist extraction with x-ray and optical imaging," Proc. SPIE **13152**, 131520Q (2024).

[63] Stock, S. R., Parker, J. T., Passerotti, M. S., Natanson, L. J., and Parkinson, D. Y., "Mineralized tissue of shark vertebral centra studied with microCT under in situ load," Proc. SPIE **13152**, 131520S (2024).

[64] Hieber, S., Bikis, C., Khimchenko, A., Schweighauser, G., Hench, J., Chicherova, N., Schulz, G., and Müller, B., "Tomographic brain imaging with nucleolar detail and automatic cell counting," Scientific Reports **6**, 32156 (2016).

[65] Nathansen, A., Clausen, M., Berning, M., MacKenzie, E., Zhang, Y., Pacureanu, A., Schaefer, A. T., Rzepka, N., and Bosch, C., "Cell nuclei segmentation in mm-scale x-ray holographic nanotomography images of mouse brain tissue," Proc. SPIE **13152**, 131521B (2024).

[66] Rau, C., Batey, D., Marathe, S., Turpin, L., Jakata, K., Cipiccia, S., Antony, I., Volpe, R., Richter, C.-P., Carriero, A., Dumoux, M., Schneider, J. E., Dall'Armellina, E., Holderied, M. W., and Van den Bulcke, J., "Hierarchical and operando tomography with x-rays and beyond," Proc. SPIE **13152**, 131521C (2024).